fluids

MDPI

Article

Experimental Study on Water Seepage Characteristics of Saturated Fragmented Coal and Rock Mass

Dingyi Hao [1], Jiaxin Huang [1], Shihao Tu [2,*] and Long Tang [2]

[1] School of Safety Science and Engineering, Anhui University of Science & Technology, Huainan 232001, China; hdycumt@163.com (D.H.); 2023200168@aust.edu.cn (J.H.)
[2] School of Mines, China University of Mining and Technology, Xuzhou 221116, China; tb22020026a41@cumt.edu.cn
* Correspondence: tsh@cumt.edu.cn

Abstract

Water inrush disasters continue to plague the advancement of deep underground mining activities. A better understanding of the structural integrity of fragmented geological bodies is crucial to ensuring mining safety. The objective of this study was to accurately reflect the dynamic evolution of pore structure changes and seepage channels in fragmented coal and rock mass of actual goafs under the coupling effect of mining stress and seepage. The co-evolution laws of the axial strain, nonlinear porosity, and permeability of fragmented coal and rock mass under different particle sizes, gradation characteristics, and stress states were compared, and a stress-pore-water seepage coupling model of the fragmented coal and rock mass was constructed. When subjected to the same axial pressure, the saturated fragmented coal exhibited a higher water permeability than the saturated fragmented rock mass. The greater the particle size, the higher the water permeability of fragmented coal and rock mass. The higher the gradation index, the higher the water permeability of these masses. Their porosity and axial pressure satisfied an exponential attenuation function, whereas their water permeability and axial pressure satisfied the Boltzmann function. The research results can provide theoretical support for preventing and controlling water inrush in goaf areas.

Keywords: fragmented coal and rock mass; water seepage; nonlinearity; porosity; permeability

1. Introduction

Water inrush disasters in goaf areas are a serious geological hazard hampering mining operations and threatening the safety of mining personnel. In essence, a water inrush is the complex migration and energy transfer process of groundwater in the discontinuous and nonuniform pore medium composed of fragmented coal and rock mass [1]. With underground coal mining moving toward even greater depths, fragmented coal and rock mass, which can be characterized as typical porous media, exhibit fractal characteristics, heterogeneity, and anisotropy in their pore structure, significantly altering the dynamic mechanism of water seepage. Under the disturbance of mining stress, such fragmented bodies contain a dynamically evolving pore network and exhibit osmotic anisotropy [2].

The seepage characteristics of water in fragmented coal and rock mass have been mostly studied through numerical simulations and laboratory experiments. For example, Wang et al. [3] constructed a cross-scale water seepage model of the pore and fracture

Academic Editor: Akira Nakayama

Received: 5 August 2025
Revised: 25 January 2026
Accepted: 7 February 2026
Published: 11 February 2026

structure of coal bodies and verified the applicability of this model. Du et al. [4] proposed an extraction method for the characteristic parameters associated with two-phase water–sand seepage in fragmented rock mass. Shuai et al. [5] numerically simulated the water seepage in a coal seam and found that the pore water pressure in the fractured area was significantly lower than that in the surrounding coal and rock mass. Zhou et al. [6] simulated the seepage characteristics of the microporous structure in coal and obtained the seepage law under low pressures. Yang et al. [7] numerically simulated and elucidated the water instep mechanism of karst collapse columns in a coal seam floor based on the variable mass seepage mechanics model. Li et al. [8] conducted seepage tests on a fragmented coal body after loading and compaction and obtained its seepage characteristics. Guo et al. [9] designed a seepage test for fragmented rock mass and analyzed the influence of particle size and stress on their porosity and permeability. Zhang et al. [10] conducted seepage experiments on fragmented mudstone and reported an increase in the permeability with increasing particle size, porosity, and water pressure. Ma et al. [11–13] conducted seepage tests on graded fragmented rock mass and obtained the influence laws of stress and gradation on their pore diameter distribution, pore fractal characteristics, and seepage behavior. Some researchers conducted seepage tests on fragmented coal and rock mass under triaxial compression [14–19]. Zhang et al. [17,18] conducted seepage experiments on graded fragmented coal and determined the mechanism of the effective stress on seepage. Li et al. [19] conducted permeability tests at different flow rates and obtained the relationship between the porosity of fragmented rock samples and the seepage velocity under different stresses.

The relationship between the void space and permeability of fragmented coal and rock mass is another important indicator that can help characterize their seepage characteristics [20–23]. Fan et al. [24] established a coupling model of stress compaction and permeability evolution and found that the rearrangement of particles can lead to the compaction of void spaces and that the permeability decreases accordingly. Shi et al. [25] constructed a nonlinear flow coupling model and obtained the evolution laws of particle migration and seepage characteristics of fragmented rock mass during seepage. Liu et al. [26] quantitatively characterized the morphological and structural changes in the fissure channels using computer graphics. Chen et al. [27] numerically simulated the injection of water into coal and rock mass and obtained the relationship between fracture parameters and shape factors. Zhang et al. [28,29] obtained the influence laws of the combination ratio and structure of coal and rock on the particle fragmentation and compaction characteristics. Ma et al. [30] conducted creep tests on fragmented rock mass and concluded that the porosity of fragmented mudstone had a negative exponential relationship with time during the creep process. Meanwhile, CT scanning and nuclear magnetic resonance techniques have also been often used to characterize the structure and void space of fragmented coal and rock mass [31–36]; these approaches have helped determine the relationship between porosity and particle size [31] and between permeability and fracture connectivity [35,36].

In summary, extensive studies have been conducted on the void space and seepage characteristics of fragmented coal and rock mass. However, there are relatively few studies that systematically compare and analyze the water seepage characteristics, such as the axial strain, porosity, and permeability, of fragmented coal and rock mass with single and graded particle sizes under different axial pressures. It remains difficult to accurately reflect the dynamic evolution of pore structure changes and infiltration channels of fragmented coal and rock mass in actual goafs under the coupling effect of mining stress and seepage. Hence, in this study, based on an analysis of the nonlinear water seepage theory applied to saturated fragmented coal and rock mass, axial loading-seepage coupling experiments were conducted on these bodies in the saturated state. The co-evolution laws of the axial

strain, porosity, and permeability were compared under different particle sizes, gradation characteristics, and stress states. Ultimately, a stress-pore-water seepage coupling model of the fragmented coal and rock mass was constructed. The results helped reveal the essence of seepage in porous media formed by water permeation disasters in goaf areas. The findings can provide theoretical support for the multiscale seepage modeling of the formation mechanism of water inundation channels in goaf areas, as well as for water prevention and control.

2. Theory of Water Seepage Characteristics in Fragmented Coal and Rock Mass

Both coal and rock mass have a strong water absorption capacity, particularly those in a fragmented state. Conducting a water seepage experiment on fragmented coal and rock mass requires immersing them in water until they reach a saturated state; a water seepage experiment can then be performed on the saturated bodies. Therefore, when studying the seepage characteristics of water in fragmented coal and rock mass, there is no need to consider the absorption effect of coal and rock mass on water.

The water seepage in a coal mine site conforms to the seepage mechanics of mining-driven rock mass established based on the seepage and loss of stability hypothesis. Common natural disasters, such as water inrush and sand collapse in coal mines, are manifestations of seepage and loss of stability. The key to this mechanism lies in the nonlinearity and parametric nature of the seepage system (i.e., the temporal variation in the parameters) [37,38]. The main mathematical basis of this hypothesis is the structural stability theory (bifurcation theory) of differential dynamical systems.

The Reynolds number of seeping water in fragmented coal and rock mass is generally much greater than 10, which goes beyond Darcy's law, and it belongs to the turbulent zone. Therefore, the seepage in a fragmented coal and rock mass is non-Darcy seepage. A non-Darcy seepage is a flow that is affected by inertial forces and turbulence and has characteristics such as a high hydraulic slope and a high Reynolds number. For non-Darcy seepage, under the same axial pressure condition (or the same porosity condition), the fluid permeability under different fluid pressures is the same; that is, due to the larger pores, the fluid pressure has no effect on the permeability.

There are many theories on non-Darcy seepage. The calculation formula in the non-Darcy seepage theory adopted herein is mainly based on the Forchheimer empirical formula ($J = av + bv^2$, 1901). The 1D momentum equation in this formula is:

$$\rho c_{wa} \frac{\partial v}{\partial t} = -\frac{\partial p}{\partial x} - \frac{\mu}{k} v - \beta \rho v^2 \tag{1}$$

For a 1D unidirectional non-Darcy steady-state water seepage in fragmented coal and rock mass, $\frac{\partial v}{\partial t} = 0$, and the above formula can be expressed as:

$$-\frac{\mathrm{d}p}{\mathrm{d}x} = \frac{\mu_w}{k_w} v_w + \beta \rho_w v_w 2 \tag{2}$$

Here, the water pressure at the outlet end is zero. Therefore, the water pressure gradient can be expressed as:

$$\frac{\mathrm{d}p}{\mathrm{d}x} = \frac{p_{w2} - p_{w1}}{h} = -\frac{p_{w1}}{h} \tag{3}$$

Combining the above two equations, we can obtain:

$$\frac{p_{w1}}{h} = \frac{\mu_{\mathrm{w}}}{k_w} v_w + \beta \rho_w v_w 2 \tag{4}$$

Here, the Darcy flow deviation factor is given by:

$$b_d = \beta \rho_w \tag{5}$$

Here, v_w is the seepage velocity of water, cm/s; μ_w is the dynamic viscosity coefficient of water, Pa·s; ρ_w represents the mass density of water; k_w is the permeability of water in the coal rock sample, mD (1 mD = 0.986923 × 10^{-15} m^2); β is a non-Darcy factor; c_{wa} is the acceleration coefficient of water; p_{w1} and p_{w2} are the water pressures at the inlet and outlet ends, respectively, MPa; and h is the sample height, cm.

For water seepage in coal and rock mass, since the flowmeter of the water seepage instrument is generally located in front of the inlet end of the coal and rock mass, and the water pressure at the outlet end is zero, let q_w be the flow rate when $p_{w1}/2$, and let q_{w1} be the flow rate at the inlet end. From the equation of state, we can obtain:

$$\frac{p_{w1}}{2} q_w = p_{w1} q_{w1} \tag{6}$$

The above equation yields:

$$q_w = 2q_{w1} = Av_w \tag{7}$$

Here, q_{w1} represents the water flow rate at the inlet end, cm^3/s, and A represents the cross-sectional area of the seepage device, cm^2.

Substituting Equation (7) into Equation (4) yields the water permeability k_w of the fragmented coal and rock mass, expressed as:

$$k_w = \frac{2\mu_w A h q_{w1}}{A^2 p_{w1} - 4\beta \rho_w h q_{w1}^2} \tag{8}$$

For non-Darcy seepage, it is necessary to perform simultaneous calculations of the flow rates under two or more different water pressures to obtain the permeability and the non-Darcy flow β factor at a particular axial pressure (or at a particular porosity). Therefore, assuming that the water pressures at the inlet end of the fragmented coal and rock mass are p_1 and p_2, respectively, while the water pressures at the outlet end are both 0, and the flow rates at the inlet end are q_1 and q_2, respectively, then the water permeability under p_1 and p_2 can be obtained as follows:

$$k_1 = \frac{2\mu_w A h q_1}{A^2 p_1 - 4\beta \rho_w h q_1^2} \tag{9}$$

$$k_2 = \frac{2\mu_w A h q_2}{A^2 p_2 - 4\beta \rho_w h q_2^2} \tag{10}$$

A comparison between Equations (9) and (10) can help obtain the non-Darcy flow β factor:

$$\beta = \frac{A^2 (q_1 p_2 - q_2 p_1)}{4\rho h (q_1 q_2^2 - q_1^2 q_2)} \tag{11}$$

After the β factor is obtained, its corresponding permeability can be determined by substituting it into Equation (9) or (10). The volume of the coal and rock mass before fragmenting and the initial volume after fragmenting are, respectively:

$$V_0 = \frac{m}{\rho} \tag{12}$$

$$V_0' = A_c h_y = \frac{\pi {d_c}^2}{4} h_y \tag{13}$$

The initial porosity of the fragmented coal and rock mass is:

$$\varphi_0 = \frac{V_0' - V_0}{V_0'} = 1 - \frac{m}{\rho A_c h_y} \tag{14}$$

During the laterally limited compaction process, the height and porosity of the fragmented coal and rock mass in different stress states can be, respectively, expressed as:

$$h = h_y - \Delta h_y \tag{15}$$

$$\varphi = 1 - \frac{m}{\rho A_c (h_y - \Delta h_y)} = 1 - \frac{4m}{\rho \pi d^2 (h_y - \Delta h_y)} \tag{16}$$

Here, m, ρ, and h_y are the mass, density, and initial height of the coal and rock sample, respectively; d_c is the inner diameter of the cylinder; V'_0 is the initial volume of the laterally compacted fragmented coal and rock mass; V_0 is the volume of the coal and rock sample before fragmenting; Δh_y is the compression height of the fragmented coal and rock mass; A_c is the cross-sectional area of the cylinder; and φ_0 is the initial porosity of the laterally compacted fragmented coal and rock mass.

3. Scheme for Water Seepage Experiments

3.1. Analysis of Mineral Components in Coal and Rock Mass

Since conducting water seepage experiments on coal and rock mass requires considering whether they contain mineral components that can react with water or are easily soluble in water, it is necessary to test and analyze these mineral components.

First, a 600-mesh (with a pore size of 25 μm) sand and gravel screen was used to screen powdered rocks and coal that met the test conditions. Subsequently, fine sandstone, medium sandstone, siltstone, and coal were detected and analyzed using an X-ray diffractometer (XRD) to obtain their corresponding mineral composition and content (as shown in Figure 1).

As shown in Figure 1, the main mineral component in siltstone, fine sandstone, and medium sandstone is quartz. Some amounts of kaolinite, muscovite, chlorite, etc., are also present. The main mineral components in the coal are coal and quartz. The weight percentages of quartz in siltstone, fine sandstone, and medium sandstone were approximately 45%, 55%, and 52%, respectively, accounting for nearly or more than half of the total. The weight percentage of the coal components in coal is approximately 67%. None of the above mineral components can react with water at normal temperature, and neither are they easily soluble. Therefore, water immersion and water seepage experiments can be conducted on siltstone, fine sandstone, medium sandstone, and coal.

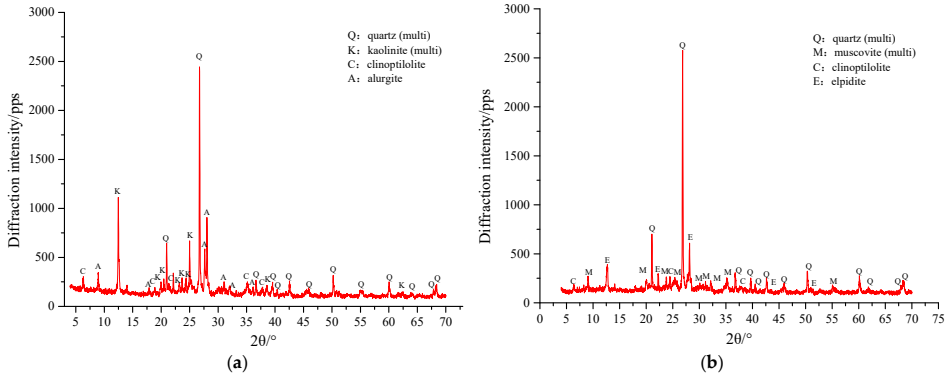

Figure 1. *Cont.*

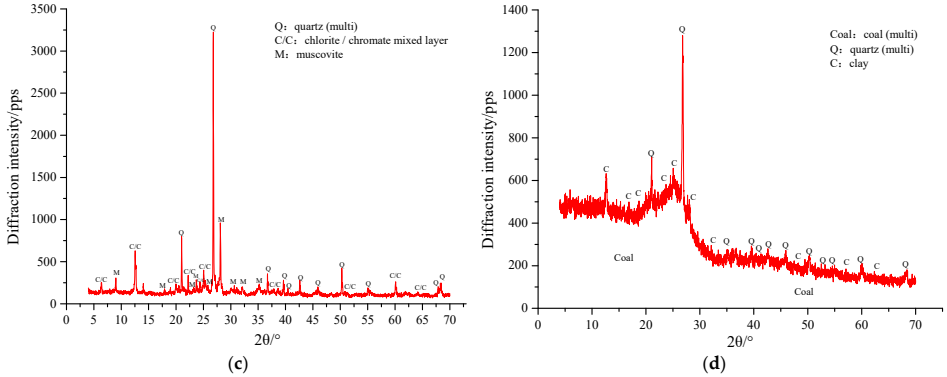

Figure 1. Main mineral components in the coal and rock mass: (**a**) siltstone; (**b**) fine sandstone; (**c**) medium sandstone; (**d**) coal.

3.2. Introduction to Instrumentation

Water seepage experiments were conducted on saturated fragmented coal and rock mass using a circulating-water-supply-type fragmented rock seepage test system. Figures 2 and 3, respectively, show the simplified device diagram and the physical device diagram. The circulating-water-supply-type fragmented rock permeability test system [39] mainly comprises four parts: an axial loading and control system, a permeation meter, a permeation pressure control system, and a data acquisition system. In terms of parameter settings, the maximum axial load, maximum axial displacement, maximum permeation pressure, and maximum permeation flow rate were set to 200 kN, 100 mm, 10 MPa, and 120 L/h, respectively. The diameter of the compaction seepage device for the fragmented rock samples was 100 mm, and the sample height was in the range of 150–200 mm.

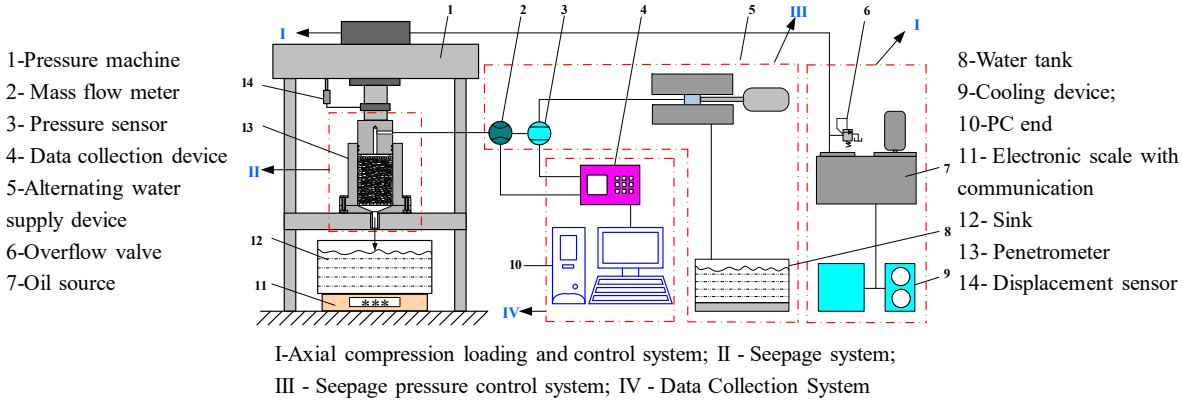

Figure 2. Simplified device diagram of the circulating-water-supply-type fragmented rock permeability test system.

This system has the following characteristics [39]: (1) It adopts an alternating water supply device, which can achieve the circulation and uninterrupted water supply of permeable water sources and can be used to study fragmented rocks with strong permeability and long pore structure adjustment cycles; (2) Through the combination of a mass flowmeter and an electronic scale, real-time collection of the lost mass can be achieved; (3) Multiple servo control systems can be set up, and corresponding control programs can be developed to achieve automatic control of the penetration test process. In addition to the aforementioned functions, other characteristics include openness, continuity, real-time performance, completeness, and simplicity.

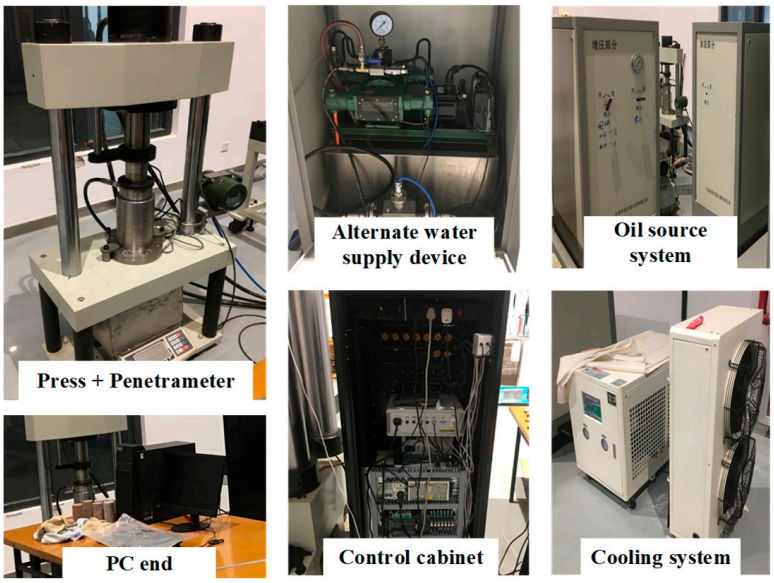

Figure 3. Physical device diagram of the circulating-water-supply-type fragmented rock permeability test system.

The following is an introduction to the two main parts of the system: the osmosis meter and the osmotic pressure control system. Figure 4 shows the permeation meter, with seepage from top to bottom. The upper permeable plate is a uniformly dense through-hole, which can evenly disperse the water flow and ensure the uniform distribution of the water pressure at the inlet end of the fragmented bodies. The lower permeable plate has large holes 10 mm in diameter, ensuring the downward migration of water during the seepage experiment on the fragmented coal and rock mass with variable mass. There is a conical surface on the base, which ensures the free flow of fine particles. As shown in Figure 5, the osmotic pressure control system adopts an alternating water supply device, including a continuous water supply pump, a servo motor, and a servo controller, which help achieve long-term and uninterrupted osmotic behavior for fragmented coal and rock mass. The key component is the continuous water supply pump, with a rated drainage pressure of 10 MPa. It can alternately fill a space with water and drain it, and the maximum water flow rate is 100 L/h. It ensures water supply and pressure for the fragmented coal and rock mass, with a rotational speed ranging from 0.1 to 1400 revolutions per minute.

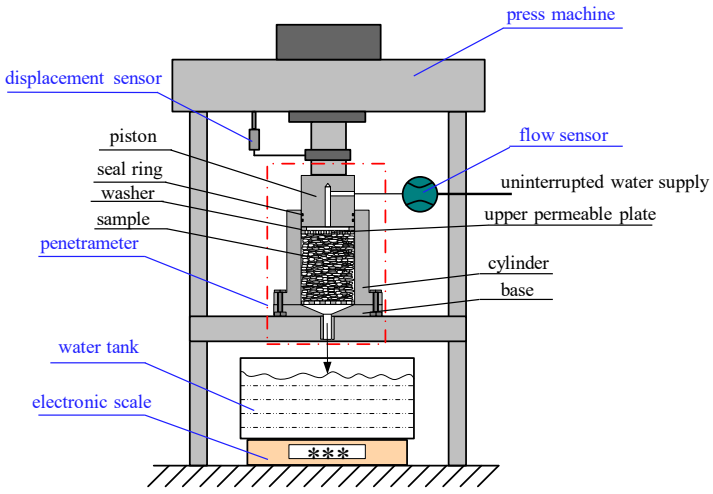

Figure 4. Press and penetrometer.

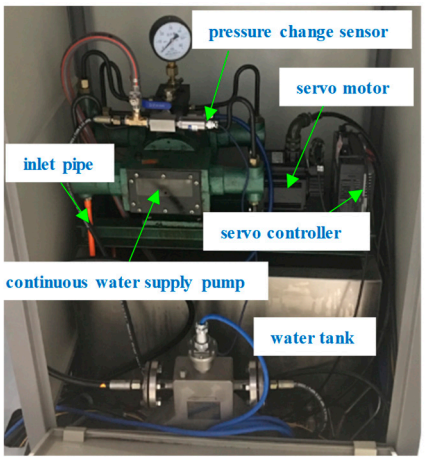

Figure 5. Alternative water supply device.

3.3. Scheme for Water Seepage Experiments in Saturated Fragmented Coal and Rock Mass

3.3.1. Water Seepage in Saturated Fragmented Rock Mass

Since the cylinder diameter shown in Figure 4 is 100 mm, the seepage mass of the saturated fragmented rock mass was 1.0 kg (the mass of the fragmented rock mass after soaking). First, a saturated fragmented rock mass of siltstone, fine sandstone, and medium sandstone weighing 1.0 kg with a single particle size range of 1.0–2.5, 2.5–5.0, and 5.0–10.0 mm was stirred evenly, and then lateral confinement compaction water seepage experiments were performed. Subsequently, the saturated fragmented rock mass of 1.0 kg of siltstone, fine sandstone, and medium sandstone with different gradations (Talbot indices of 0.1, 0.2, 0.4, 0.6, and 0.8) was uniformly stirred, and lateral confinement compaction water seepage experiments were conducted. According to the Talbot grading formula (as shown in Equation (17)), the particle size distribution can be calculated as shown in Table 1. Based on the designed stress loading path, loading and seepage experiments were performed on the saturated fragmented rock mass, thus obtaining the water seepage characteristics of the saturated fragmented rock mass with single and graded particle sizes during the confined compaction process.

$$P_i = \left(\frac{d_i}{d_M}\right)^n \times 100\% \quad (17)$$

Table 1. Particle size distribution of rock samples with different initial ratios.

Talbot Index	Quality/g		
	1.0~2.5 mm	2.5~5.0 mm	5.0~10.0 mm
0.1	370.6	303.8	325.6
0.2	343.9	305.4	350.8
0.4	292.8	304.9	402.3
0.6	245.8	299.8	454.4
0.8	203.7	290.5	505.8

Here, d_i and d_M are the particle size and maximum particle size of rock particles, respectively, in mm; n is the Talbot power index; and P_i is the mass fraction of rock particles, the size of which is less than or equal to d_i in the rock sample.

3.3.2. Water Seepage in Saturated Fragmented Coal

Since coal has a lower bulk density than the rock mass, coal of the same volume is significantly lighter than rock, and coal is a porous medium. The pore and fracture medium is also more complex. Therefore, the seepage mass of the saturated fragmented coal was

set to 500 g. First, after uniformly stirring 500 g of saturated fragmented coal with a single particle size range of 1.0–2.5, 2.5–5.0, and 5.0–10.0 mm, the lateral confinement compaction water seepage experiment was conducted. Subsequently, side-limiting compaction water seepage experiments were conducted on the saturated fragmented coal weighing 500 g with different gradations (Talbot indices were 0.1, 0.2, 0.4, 0.6, and 0.8) after thorough stirring; Table 2 presents the particle size distribution. Based on the designed stress loading path, loading and seepage experiments were conducted on the saturated fragmented coal body. Thus, the water seepage characteristics of the saturated fragmented coal body with single and graded particle sizes during the confined compaction process were obtained.

Table 2. Particle size distribution of coal samples with different initial proportioning.

Talbot Index	Quality/g		
	1.0~2.5 mm	**2.5~5.0 mm**	**5.0~10.0 mm**
0.1	185.3	151.9	162.8
0.2	171.9	152.7	175.4
0.4	146.4	152.4	201.2
0.6	122.9	149.9	227.2
0.8	101.8	145.3	252.9

3.4. Stress Loading Path for Water Seepage in Saturated Fragmented Coal and Rock Mass

During the water seepage experiment on the fragmented coal and rock mass, a 40-mesh metal filter screen with an extremely fine pore size was placed at the bottom of the fragmented coal and rock mass to avoid any mass loss. In other words, this study did not consider the phenomenon of mass change in the fragmented coal and rock mass caused by the migration and loss behavior of the fine particles inside these bodies. Figure 6 shows the specific test process for the seepage characteristics of the side-confined compacted water in the fragmented coal and rock mass. During the experiment, the loading speed of the axial pressure was kept the same. After the axial pressure load was stabilized, water seepage experiments were conducted at different water pressures. Figure 7 shows the specific stress loading path for water seepage in the fragmented coal and rock mass.

Meanwhile, the fragmented coal and rock mass were saturated and soaked to prevent them from absorbing a large amount of water during the water seepage experiment. The fragmented coal and rock masses of different particle sizes were soaked until their quality no longer changed significantly within 24 h, indicating these masses were saturated with water. Thereafter, the water seepage experiment was conducted. Figure 8 presents the saturated moisture content in the fragmented coal and rock mass with different particle sizes. As shown, the larger the particle size, the worse the water absorption and the lower the saturated water content. The saturated water content of the coal and rock mass with the same particle size followed the order: coal > siltstone > fine sandstone > medium sandstone. The coal body had a stronger water absorption than the rock mass, and the smaller the particle size of the rock matrix, the stronger the water absorption.

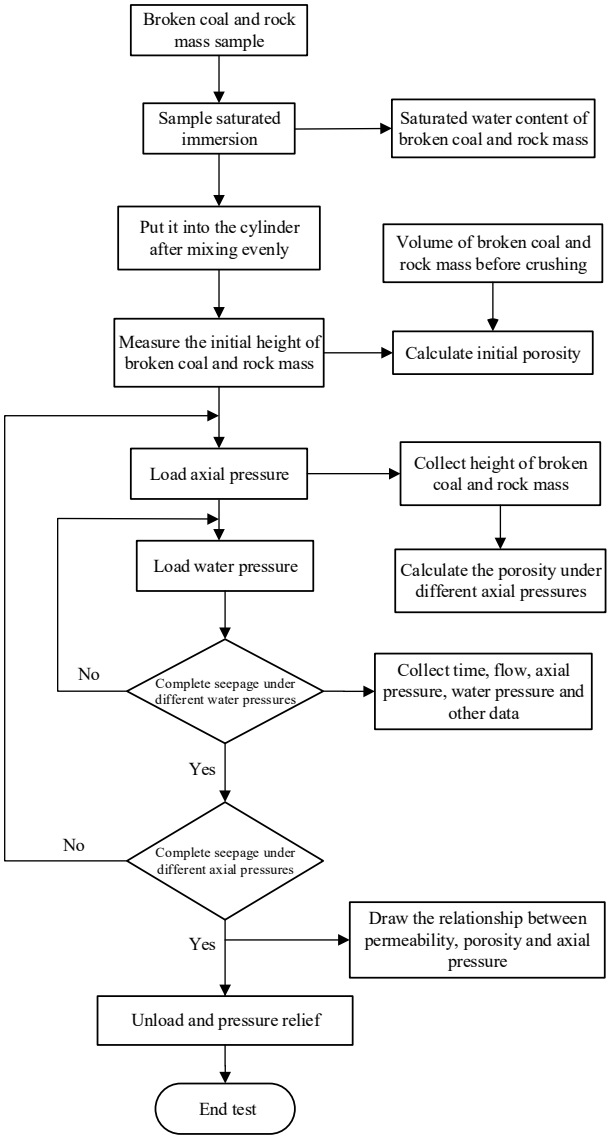

Figure 6. Testing process of the seepage characteristics of confined compacted water in fragmented coal and rock.

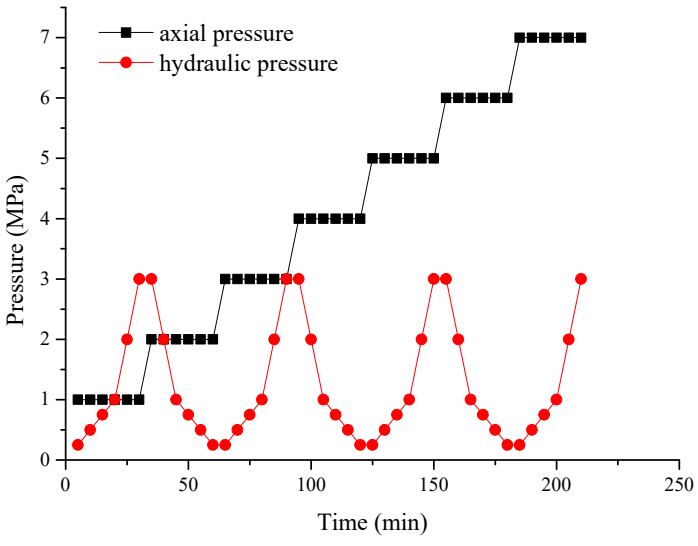

Figure 7. Stress loading path for water seepage into fragmented coal and rock.

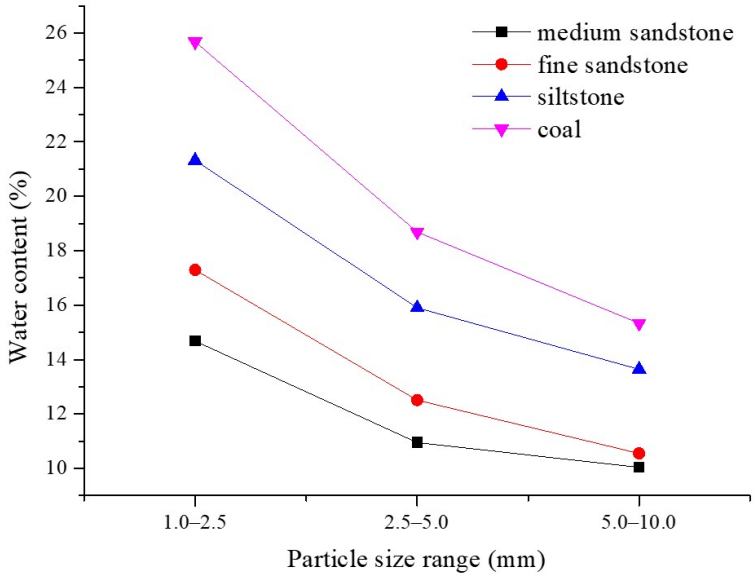

Figure 8. Saturated water content of fragmented coal and rock with different particle sizes.

4. Experimental Results and Analysis

Saturated water seepage experiments were conducted on fragmented coal and rock mass with single and graded particle sizes under lateral confinement compaction conditions. The co-evolution laws of the axial strain, porosity, and permeability of these bodies were compared and analyzed. With the results obtained, a stress-pore-water seepage coupling model of the fragmented coal and rock mass was constructed.

4.1. Water Seepage Characteristics in Saturated Fragmented Rock Mass with a Single Particle Size

Figure 9 shows the variation law of the axial strain of the saturated fragmented rock mass with a single particle size under the effect of water seepage. As shown, with increasing axial pressure, the axial strain gradually increases, with the increase in amplitude gradually decreasing. The greater the particle size, the greater the axial strain of the laterally compacted saturated fragmented rock mass. That is, the lower the particle size, the more difficult it is to compact this type of rock mass. Because the compressive strength of the fragmented rock mass reduced after saturated soaking, the axial strain of the laterally compacted saturated fragmented rock mass with a single particle size was greater than that of the common single-particle-size fragmented rock mass.

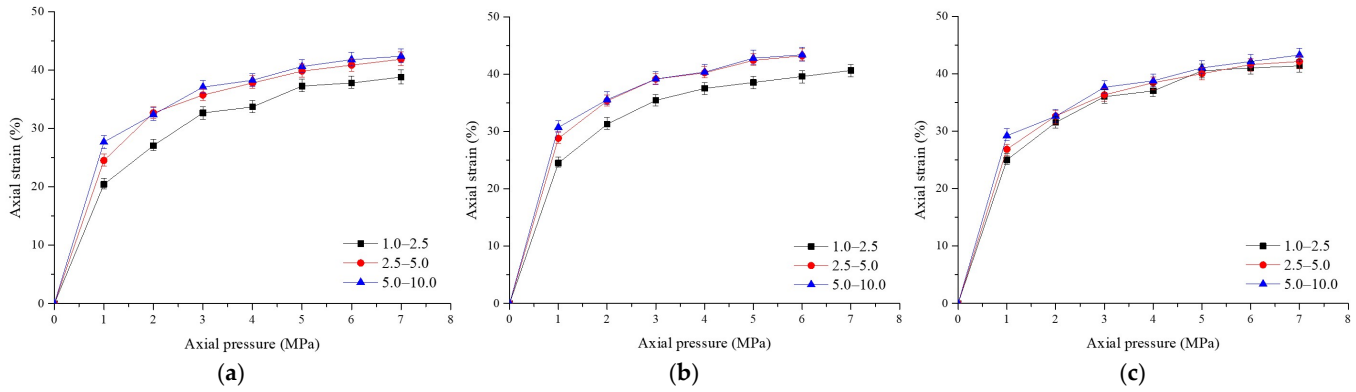

Figure 9. Axial strain of the saturated fragmented rock with a single particle size under the effect of water seepage: (**a**) siltstone; (**b**) fine sandstone; (**c**) medium sandstone.

The porosity of the saturated fragmented coal and rock mass was calculated using Equation (16). Figure 10 shows the variation law of the porosity of the saturated fragmented

rock mass with a single particle size under the effect of water seepage. As shown, with increasing axial pressure, the porosity of the laterally compacted single-particle-size saturated fragmented rock mass gradually decreased, with the reduction amplitude gradually decreasing. The larger the particle size, the greater the porosity of the laterally compacted saturated fragmented rock mass. The initial porosity of the saturated fragmented rock mass was in the range of 45–50%, slightly lower than that of the ordinary fragmented rock mass with a single particle size. Moreover, after axial pressure loading, due to the reduced strength, the degree of porosity reduction was significantly greater than that of the ordinary fragmented rock mass. When the axial pressure was increased to 7 MPa, the porosity of the saturated fragmented rock mass with a single particle size decreased to approximately 10%.

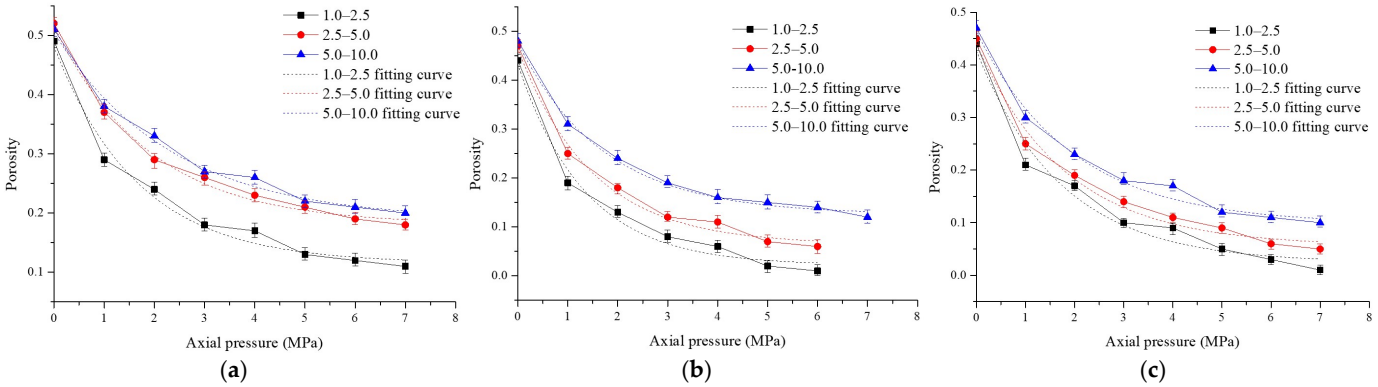

Figure 10. Porosity of a saturated fragmented rock with a single particle size under the effect of water seepage: (**a**) siltstone; (**b**) fine sandstone; (**c**) medium sandstone.

The porosity and axial pressure of the single-particle-size saturated fragmented rock mass under the effect of water seepage, shown in Figure 10, were fitted, and these parameters were found to satisfy an exponential attenuation function. The specific fitting formula is expressed as in Equation (18); Table 3 presents the related fitting parameters and fitting degrees.

$$\varphi = m_1 + u_1 e^{\frac{-\sigma_a}{v_1}} \quad (18)$$

Table 3. Parameters and fitting degree of the porosity-axial pressure fitting curves of saturated fragmented rock mass with a single particle size.

Lithology	Particle Size Range/mm	Fitting Parameters			Fitting Degree
		m_1	u_1	v_1	R^2
Siltstone	1.0–2.5	0.1152	0.3662	1.6771	0.9800
	2.5–5.0	0.1804	0.3353	1.8979	0.9929
	5.0–10.0	0.1876	0.3172	2.3279	0.9895
Fine sandstone	1.0–2.5	0.0217	0.4111	1.3417	0.9783
	2.5–5.0	0.0643	0.4004	1.4855	0.9873
	5.0–10.0	0.1255	0.3508	1.7135	0.9951
Medium sandstone	1.0–2.5	0.0239	0.4029	1.7299	0.9658
	2.5–5.0	0.0557	0.3846	1.8081	0.9826
	5.0–10.0	0.0976	0.3654	1.9615	0.9859

Here, σ_a represents the axial pressure of the fragmented coal and rock mass, and m_1, u_1, and v_1 are the fitting parameters.

Figure 11 shows the variation law of the permeability of the saturated fragmented rock mass with a single particle size under the effect of water seepage. Since the water seepage experiment was conducted at room temperature, a water permeation viscosity coefficient of 100.5×10^{-5} Pa·s at 20 °C was adopted for the permeability calculations. Figure 11

shows that with axial pressure loading, the water permeability of the saturated fragmented rock mass with a single particle size gradually decreases, with the reduction amplitude gradually decreasing. After the axial pressure was increased to a certain value, water almost no longer permeated. The greater the particle size, the larger the pores between the saturated fragmented rock mass, resulting in a higher water permeability. When the axial pressure was relatively low, the order of the water permeability of the saturated fragmented rock mass with a single particle size was 10^2 mD.

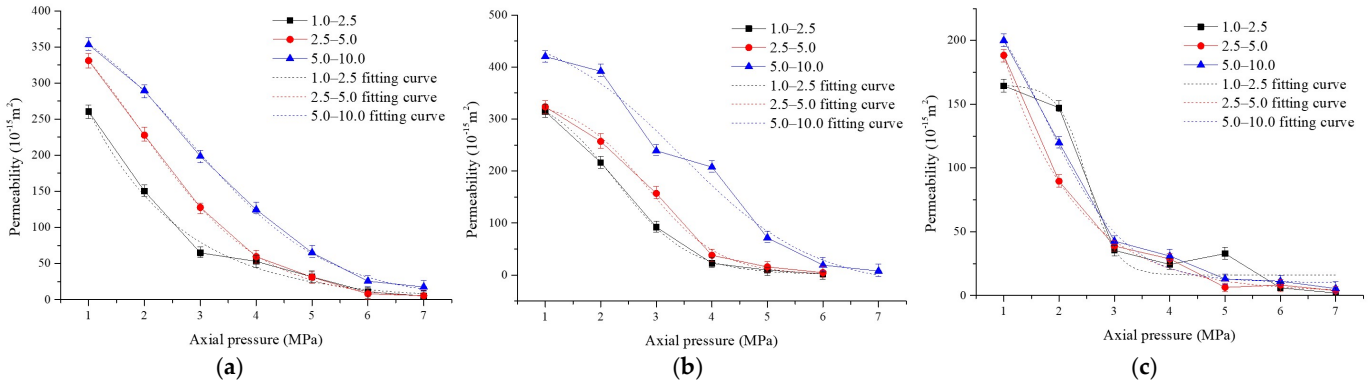

Figure 11. Permeability of a single-particle-size saturated fragmented rock under the effect of water seepage: (**a**) siltstone; (**b**) fine sandstone; (**c**) medium sandstone.

The water permeability and axial pressure of the single-particle-size saturated fragmented rock mass, shown in Figure 11, were fitted and were found to satisfy the Boltzmann function. The specific fitting formula is expressed as in Equation (19). Table 4 presents the related fitting parameters and fitting degree.

$$k_w = \frac{u_2 - v_2}{1 + e^{(\sigma_a - m_2)/n_2}} + v_2 \quad (19)$$

Table 4. Parameters and fitting degree of the water permeability-axial pressure fitting curves for single-particle-size saturated fragmented rock.

Lithology	Particle Size Range/mm	Fitting Parameters				Fitting Degree
		u_2	v_2	m_2	n_2	R^2
Siltstone	1.0–2.5	53,953.9004	1.0298	−7.8825	1.6667	0.9843
	2.5–5.0	478.8366	0.3929	1.8871	1.0991	0.9993
	5.0–10.0	432.1248	0.5691	2.8416	1.2255	0.9987
Fine sandstone	1.0–2.5	359.3898	1.5542	2.2732	0.6587	0.9994
	2.5–5.0	338.9554	0.6095	2.8282	0.6497	0.9919
	5.0–10.0	486.0133	−25.5660	3.4468	1.2007	0.9578
Medium sandstone	1.0–2.5	164.9726	16.0903	2.5134	0.2594	0.9529
	2.5–5.0	48,767.0330	2.6480	−6.2556	1.3033	0.9927
	5.0–10.0	267.7869	10.1769	1.7546	0.7261	0.9895

Here, σ_a represents the axial pressure of the saturated fragmented coal and rock mass, and u_2, v_2, m_2, and n_2 are the fitting parameters.

4.2. Water Seepage Characteristics in Saturated Fragmented Rock Mass with Graded Particle Size

Figure 12 shows the variation law of the axial strain of the saturated fragmented rock mass with a graded particle size under the effect of water seepage. Clearly, with increasing axial pressure, the axial strain gradually increased, with the increase in amplitude gradually decreasing. The increase in the gradation index did not have a certain pattern of influence on the axial strain of the saturated fragmented rock mass. Compared with the common

graded-particle-size fragmented rock mass, the graded saturated fragmented rock mass exhibited a higher lateral compaction axial strain due to the water-saturated soaking of the rock.

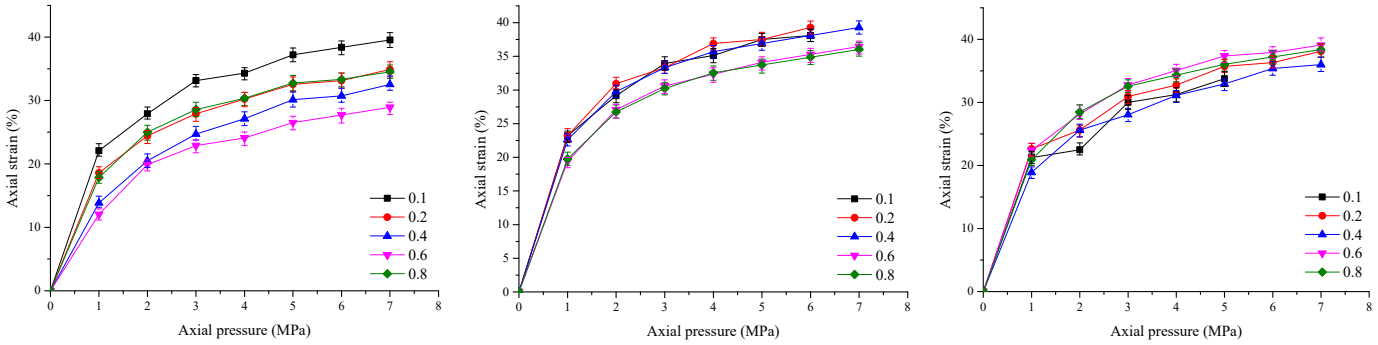

(**a**) (**b**) (**c**)

Figure 12. Axial strain of the graded saturated fragmented rock under the effect of water seepage: (**a**) siltstone; (**b**) fine sandstone; (**c**) medium sandstone.

Figure 13 shows the variation law of the porosity of the saturated fragmented rock mass with a graded particle size under the effect of water seepage. Clearly, with increasing axial pressure, the porosity gradually decreased, with the reduction amplitude gradually decreasing. The increase in the gradation index did not show a certain pattern in its influence on the porosity. Compared with the fragmented rock mass with a common graded particle size, the graded saturated fragmented rock mass exhibited a higher lateral compaction porosity due to the water-saturated soaking of the rock. The initial porosity of the saturated fragmented rock mass with a graded particle size was approximately 40% to 45%, slightly lower than that of the ordinary fragmented rock mass with a graded particle size. After axial pressure loading, due to the weakening of the saturated fragmented rock mass, the degree of porosity reduction was greater than that of the ordinary fragmented rock mass. Compared with saturated fragmented rock mass having a single particle size, graded-particle-size saturated fragmented rock mass exhibited relatively lower initial porosity. When the axial pressure was increased to 7 MPa, the porosity of the saturated fragmented rock mass with a graded particle size decreased to approximately 10%. The exponential attenuation function, expressed in Equation (18), was used to fit the porosity and axial pressure of the graded saturated fragmented rock mass under the effect of water seepage. Table 5 presents the corresponding fitting parameters and fitting degrees.

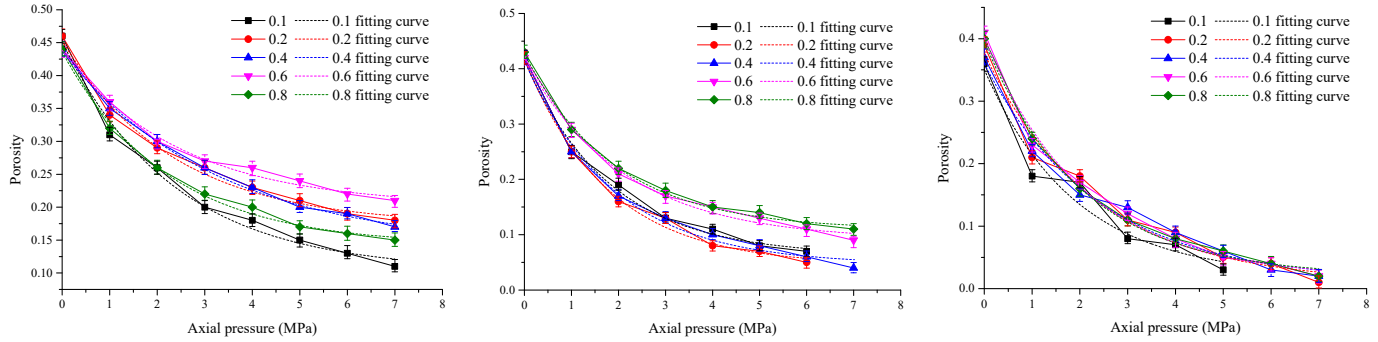

(**a**) (**b**) (**c**)

Figure 13. Porosity of a graded saturated fragmented rock under the effect of water seepage: (**a**) siltstone; (**b**) fine sandstone; (**c**) medium sandstone.

Table 5. Parameters and fitting degree of the porosity axial pressure fitting curves of saturated fragmented rock mass with a graded particle size.

Lithology	Talbot Index	Fitting Parameters			Fitting Degree
		m_1	u_1	v_1	R^2
Siltstone	0.1	0.1034	0.3482	2.3569	0.9867
	0.2	0.1729	0.2803	2.3284	0.9884
	0.4	0.1399	0.2965	3.2323	0.9969
	0.6	0.2021	0.2363	2.4779	0.9910
	0.8	0.1419	0.2942	2.2003	0.9953
Fine sandstone	0.1	0.0623	0.3531	1.8096	0.9918
	0.2	0.0445	0.3726	1.7752	0.9937
	0.4	0.0456	0.3686	1.8927	0.9915
	0.6	0.0906	0.3264	2.1095	0.9932
	0.8	0.1088	0.3181	1.9149	0.9964
Medium sandstone	0.1	0.0196	0.3311	1.8913	0.9324
	0.2	0.0089	0.3675	2.2948	0.9687
	0.4	0.0113	0.3483	2.3787	0.9785
	0.6	0.0172	0.3838	2.0748	0.9879
	0.8	0.0195	0.3759	2.0506	0.9952

Figure 14 shows the variation law of the permeability of the saturated fragmented rock mass with a graded particle size under the effect of water seepage. Clearly, with increasing axial pressure loading, the water permeability gradually decreased, with the reduction amplitude gradually decreasing. After the axial pressure was increased to a certain value, there was almost no seepage. When the axial pressure was relatively low, the order of the water permeability was 10^2 mD. The higher the gradation index, the higher the water permeability of the saturated fragmented rock mass. In other words, the greater the proportion of the large-particle saturated fragmented rock mass, the higher the water permeability. The Boltzmann function, expressed in Equation (19), was used to fit the water permeability and axial pressure of the saturated fragmented rock mass with a graded particle size. Table 6 presents the corresponding fitting parameters and fitting degrees.

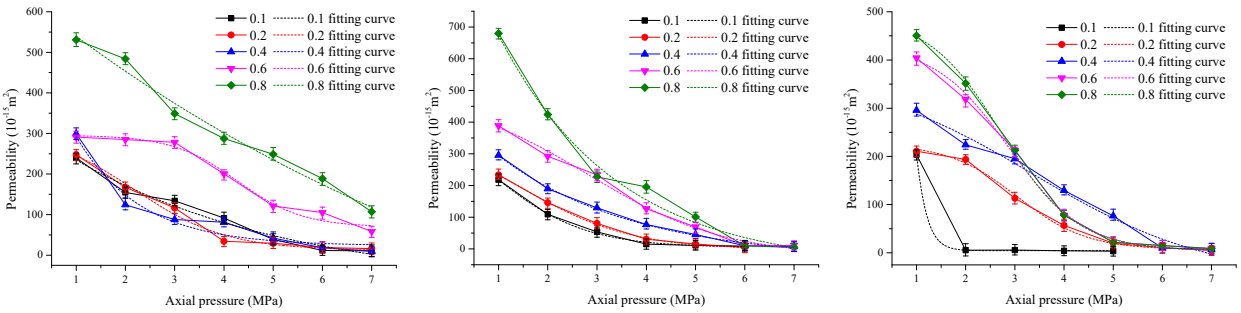

Figure 14. Water seepage permeability of graded saturated fragmented rock: (**a**) siltstone; (**b**) fine sandstone; (**c**) medium sandstone.

Table 6. Parameters and fitting degree of water permeability-axial pressure fitting curves for graded saturated fragmented rock.

Lithology	Talbot Index	Fitting Parameters				Fitting Degree
		u_2	v_2	m_2	n_2	R^2
Siltstone	0.1	9731.4979	−75.9124	−13.6105	4.2719	0.9595
	0.2	311.6512	12.5459	2.1765	0.9378	0.9749
	0.4	1.0769×10^6	23.1161	−9.8386	1.3068	0.9307
	0.6	295.8909	69.1667	4.2758	0.6651	0.9709
	0.8	29,611.5539	−480.4286	−35.7297	10.9637	0.9665

Table 6. *Cont.*

Lithology	Talbot Index	Fitting Parameters				Fitting Degree
		u_2	v_2	m_2	n_2	R^2
Fine sandstone	0.1	485.5012	4.7482	0.7823	0.9646	0.9946
	0.2	391.9450	−2.2556	1.4447	1.1251	0.9979
	0.4	37,783.1528	−35.0068	−12.0329	2.7525	0.9952
	0.6	492.3865	−23.0825	2.8185	1.3915	0.9867
	0.8	528,808.0333	−56.1099	−14.8705	2.4108	0.9778
Medium sandstone	0.1	1150.0747	4.4637	0.7104	0.1857	0.9996
	0.2	226.2389	6.5142	3.0510	0.7058	0.9928
	0.4	379.9336	−54.3174	3.3779	1.8102	0.9738
	0.6	432.7393	3.9292	2.8784	0.7611	0.9949
	0.8	493.0016	4.8510	2.7281	0.7581	0.9982

4.3. Water Seepage Characteristics in Saturated Fragmented Coal with a Single Particle Size

Figure 15 shows the seepage characteristics of water in a saturated fragmented coal with a single particle size. Clearly, with increasing axial pressure, the axial strain gradually increased, with its increase in amplitude gradually decreasing. Both the porosity and permeability gradually decreased, with their reduction amplitudes gradually decreasing. The greater the particle size, the greater the axial strain of the laterally compacted saturated fragmented coal body, the greater the porosity, and the greater the permeability. This indicates that the greater the particle size, the easier it is to compact the saturated fragmented coal body. The initial porosity of the saturated fragmented coal with a single particle size was approximately in the range of 45–50%. After compaction, its porosity decreased to approximately 15%. Compared with the ordinary fragmented coal with a single particle size, due to water saturation soaking, which weakens the coal, the saturated fragmented coal with a single particle size after lateral limiting compaction exhibited a higher axial strain and a lower porosity. Compared with the saturated fragmented rock mass with a single particle size, the permeability of the saturated fragmented coal body with a single particle size was still relatively high when the axial pressure was increased to 7 MPa, and the order of the water permeability was still 10^2 mD. The exponential attenuation function expressed in Equation (18) and the Boltzmann function, expressed in Equation (19), were, respectively, used to fit the porosity and axial pressure of the saturated fragmented coal with a single particle size under the effect of seepage, as well as the permeability and axial pressure of water. Tables 7 and 8 present the corresponding fitting parameters and fitting degrees, respectively.

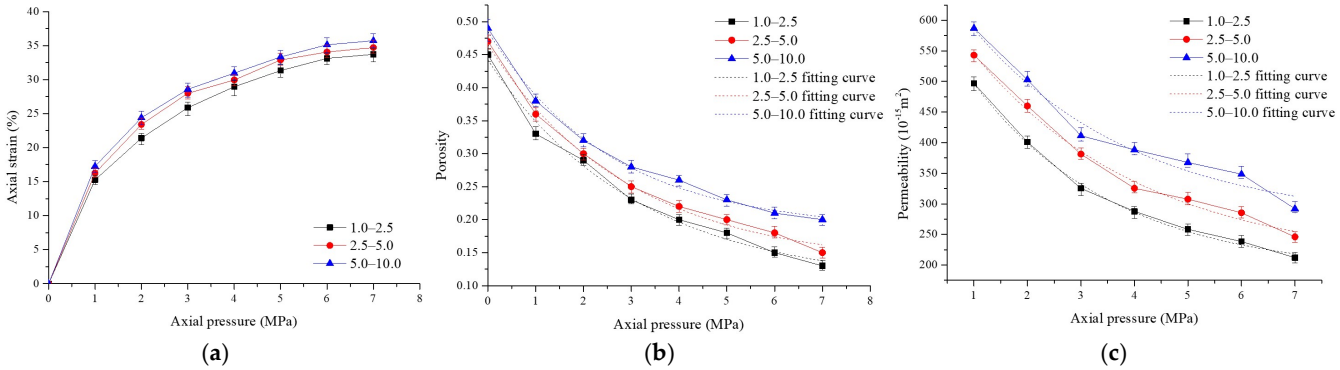

Figure 15. Water seepage characteristics of single-size saturated fragmented coal: (**a**) axial strain; (**b**) porosity; (**c**) permeability.

Table 7. Parameters and fitting degree of the porosity-axial pressure fitting curves for single-particle-size saturated fragmented coal.

Lithology	Particle Size Range/mm	Fitting Parameters			Fitting Degree
		m_1	u_1	v_1	R^2
coal	1.0–2.5	0.1010	0.3409	3.1375	0.9883
	2.5–5.0	0.1311	0.3342	2.9326	0.9938
	5.0–10.0	0.1848	0.3006	2.5721	0.9941

Table 8. Parameters and fitting degree of the water permeability-axial pressure curves for single-particle-size saturated fragmented coal.

Lithology	Particle Size Range/mm	Fitting Parameters				Fitting Degree
		u_2	v_2	m_2	n_2	R^2
coal	1.0–2.5	103,156.8812	185.9579	−14.3426	2.6451	0.9956
	2.5–5.0	24,851.2569	203.4457	−12.4375	3.1501	0.9864
	5.0–10.0	228,439.8915	268.5815	−18.9799	3.0375	0.9507

4.4. Water Seepage Characteristics in Saturated Fragmented Coal with Graded Particle Size

Figure 16 shows the seepage characteristics of the saturated fragmented coal with a graded particle size. Clearly, with increasing axial pressure, the axial strain gradually increased, with the increase in amplitude gradually decreasing. Both the porosity and permeability gradually decreased, with their reduction amplitudes gradually decreasing. The greater the gradation index, the greater the number of large-particle saturated fragmented coal bodies. Therefore, the axial strain, porosity, and permeability of the laterally confined compacted body were higher. The initial porosity of the saturated fragmented coal with a graded particle size was in the range of 40–45%. After compaction, its porosity decreased to approximately 10%. Compared with the ordinary fragmented coal with a graded particle size, due to water saturation soaking, which weakens the coal, the saturated fragmented coal with a graded particle size after lateral limiting compaction exhibited a greater axial strain and a lower porosity. Compared with the saturated fragmented coal having a single particle size, the saturated fragmented coal bodies composed of different graded particle sizes exhibited a lower porosity (the initial porosity and post-compaction porosity were relatively low) and a lower water permeability under the same axial pressure. Compared with the saturated fragmented rock mass with a graded particle size, the saturated fragmented coal with a graded particle size continued to exhibit a relatively high permeability even when the axial pressure was increased to 7 MPa, and the order of the water permeability was still 10^2 mD. The porosity and axial pressure of the saturated fragmented coal with a graded particle size under the effect of seepage, as well as the water permeability and axial pressure, were fitted using the exponential attenuation function (Equation (18)) and the Boltzmann function (Equation (19)), respectively. Tables 9 and 10 present the corresponding fitting parameters and fitting degrees, respectively.

Table 9. Parameters and fitting degree of the porosity-axial pressure fitting curves of graded-particle-size saturated fragmented coal.

Lithology	Talbot Index	Fitting Parameters			Fitting Degree
		m_1	u_1	v_1	R^2
coal	0.1	0.0769	0.2997	1.7612	0.9453
	0.2	0.0882	0.2799	1.3932	0.9938
	0.4	0.0906	0.3264	2.1095	0.9932
	0.6	0.1034	0.3482	2.3569	0.9867
	0.8	0.1419	0.2942	2.2003	0.9953

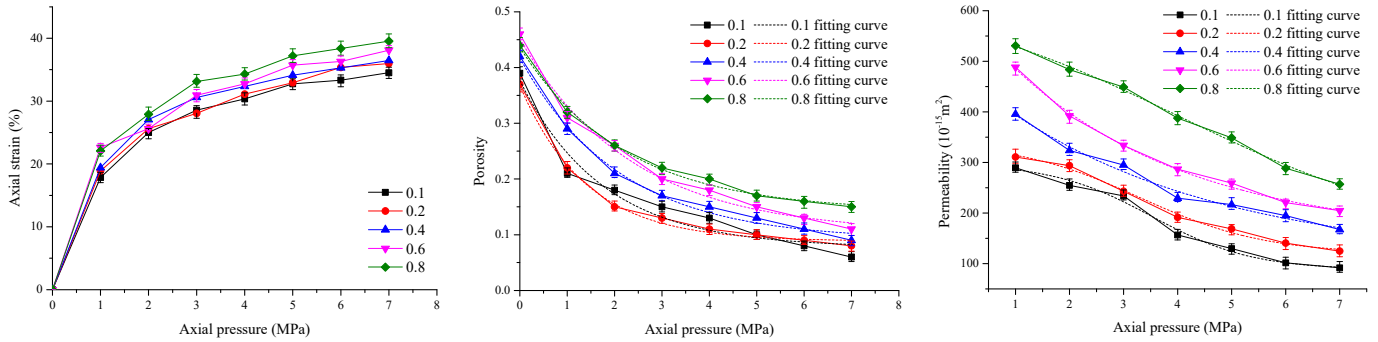

Figure 16. Water seepage characteristics of graded saturated fragmented coal: (**a**) axial strain; (**b**) porosity; (**c**) permeability.

Table 10. Parameters and fitting degree of the water permeability-axial pressure fitting curve for graded-particle-size saturated fragmented coal.

Lithology	Talbot Index	Fitting Parameters				Fitting Degree
		u_2	v_2	m_2	n_2	R^2
coal	0.1	298.8511	88.0692	3.5219	0.9313	0.9794
	0.2	341.0942	119.3887	3.3099	1.1612	0.9889
	0.4	30,515.6709	105.1527	−17.7606	4.0367	0.9757
	0.6	114,134.1089	152.8468	−18.0800	3.2708	0.9956
	0.8	639.5872	140.3227	4.0525	2.4332	0.9939

Through the above series of water seepage experiments on the saturated fragmented coal and rock mass and data fitting, it can be concluded that the porosity and axial pressure, as well as the water permeability and axial pressure, all satisfied the exponential attenuation function expressed in Equation (18) and the Boltzmann function expressed in Equation (19). By combining these equations, Equation (20) can be obtained, which is the coupled model of the stress-pore-water seepage for saturated fragmented coal and rock mass. When conducting numerical simulations on water seepage in saturated fragmented coal and rock mass with different particle sizes or gradations, the corresponding fitting parameters can be found, respectively, from Tables 3–10.

$$\begin{cases} \varphi = m_1 + u_1 e^{\frac{-\sigma_a}{v_1}} \\ k_w = \frac{u_2 - v_2}{1 + e^{(\sigma_a - m_2)/n_2}} + v_2 \end{cases} \quad (20)$$

5. Conclusions

In this study, axial loading-seepage coupling experiments were conducted on fragmented coal and rock mass in a saturated state based on the nonlinear water seepage theory. The co-evolution laws of the axial strain, porosity, and permeability of fragmented coal and rock mass under different particle sizes, gradation characteristics, and stress states were compared, and a stress-pore-water seepage coupling model was constructed. The main conclusions are as follows:

(1) Based on Darcy's law and Forchheimer's empirical formula employed in the non-Darcy seepage theory, and combined with the characteristics of the water seepage instrument employed for testing coal and rock mass, a nonlinear water permeability expression for fragmented coal and rock mass was derived. The main mineral components in the coal and rock mass were analyzed. The main mineral component in the rock mass was identified to be quartz, and the main mineral components in the coal body were coal and quartz.

(2) Combined with the characteristics of the circulating-water-supply-type fragmented rock permeability test system, the test process, stress loading path, and other experimental schemes were designed to determine the water seepage characteristics of saturated fragmented coal and rock mass. Water saturation immersion experiments were conducted on fragmented coal and rock mass with different particle sizes, and their saturated moisture contents were obtained. The greater the particle size, the lower the saturated moisture content. The order of the saturated moisture content of the fragmented coal and rock mass with the same particle size was as follows: coal > siltstone > fine sandstone > medium sandstone.

(3) The water seepage characteristics of the saturated fragmented coal and rock mass with different particle sizes and gradations were obtained, and a stress-pore-water seepage coupling model was constructed. With increasing axial pressure, the water permeability gradually decreased, with the reduction amplitude gradually decreasing. The larger the particle size, the greater the water permeability. When subjected to the same axial pressure, the saturated fragmented coal exhibited a higher water permeability than the saturated fragmented rock mass. The higher the gradation index, the higher the water permeability of the saturated fragmented coal and rock mass. The porosity and axial pressure of the saturated fragmented coal and rock mass satisfied the exponential attenuation function, whereas the water permeability and axial pressure satisfied the Boltzmann function.

Author Contributions: Conceptualization, D.H.; methodology, D.H.; software, D.H.; validation, D.H.; formal analysis, J.H.; investigation, L.T.; resources, S.T.; data curation, J.H.; writing—original draft preparation, D.H.; writing—review and editing, S.T.; visualization, L.T.; supervision, S.T.; project administration, D.H.; funding acquisition, D.H. All authors have read and agreed to the published version of the manuscript.

Funding: This research was funded by the National Natural Science Foundation of China (U23A20601, 52204123).

Institutional Review Board Statement: Not applicable.

Informed Consent Statement: Not applicable.

Data Availability Statement: The data generated and/or analyzed during this study are available from the corresponding author on reasonable request.

Conflicts of Interest: The authors declare no conflicts of interest.

References

1. Xie, H. Research review of the state key research development program of China: Deep rock mechanics and mining theory. *J. China Coal Soc.* **2019**, *44*, 1283–1305.
2. Zhang, T.; Xie, Z.; Yuan, L.; Tang, M.; Zheng, K.; Zhang, C.; Mao, J. Study on coal damage and pore-fracture evolution ahead of the mining face under the disturbance of coal mining. *J. China Coal Soc.* **2024**, *49*, 981–994.
3. Wang, G.; Wang, S.; Li, H.; Qin, X.; Li, S. Study on water phase seepage evolution model considering mesoscale characteristics of pore and fissure in coal. *Chin. J. Rock Mech. Eng.* **2021**, *40*, 1547–1558.
4. Du, F.; Cao, Z.; Li, Z. Research progress of two phase water-sand flow characteristics in crushed rock mass. *Coal Sci. Technol.* **2018**, *46*, 48–53.
5. Shuai, G.; Zhang, Y.; Zheng, X.; Chen, J.; Zhang, Z.; Zhao, X. Simulation of dual-porosity medium seepage flow in fractured zone. *Coal Sci. Technol.* **2019**, *47*, 145–150.
6. Zhou, G.; Zhang, Q.; Bai, R.; Ni, G. Characterization of Coal Micro-Pore Structure and Simulation on the Seepage Rules of Low-Pressure Water Based on CT Scanning Data. *Miner* **2016**, *6*, 78. [CrossRef]
7. Yang, F.; Lin, H.; Shen, L.; Yan, A.; Wu, Y. Water Inrush Mechanism of Karst Collapse Column in Coal Seam Floor Based on a Variable Mass Seepage Mechanical Model. *Geofluids* **2022**, *2022*, 8148203. [CrossRef]

8. Li, B.; Liang, Y.; Zhang, L.; Zhou, Q. Edited and approved by editor experimental investigation on compaction characteristics and permeability evolution of broken coal. *Int. J. Rock Mech. Min. Sci.* **2019**, *118*, 63–76. [CrossRef]
9. Guo, Y.; Zhang, J.; Li, M.; Wang, L.; Li, Z. Preventing water inrush hazards in coal mines by coal gangue backfilling in gobs: Influences of the particle size and stress on seepage characteristics. *Environ. Sci. Pollut. Res.* **2023**, *30*, 104374–104387. [CrossRef] [PubMed]
10. Zhang, B.; Lin, Z. Seepage property of crushed mudstone rock in collapse column. *Adv. Civ. Eng.* **2020**, *2020*, 8866697. [CrossRef]
11. Ma, D.; Li, Q.; Zhang, J.; Liu, Y.; Hou, W. Pore structure characterization and nonlinear seepage characteristics of rock mass in fault fracture zones. *J. China Coal Soc.* **2023**, *48*, 666–677.
12. Ma, D.; Miao, X.; Wu, Y.; Bai, H.; Wang, J.; Rezania, M.; Huang, Y.; Qian, H. Seepage properties of crushed coal particles. *J. Petrol. Sci. Eng.* **2016**, *146*, 297–307.
13. Ma, D.; Miao, X.; Jiang, H.; Bai, H.; Chen, Z. An Experimental Investigation of Permeability Measurement of Water Flow in Crushed Rocks. *Transp. Porous Media* **2014**, *105*, 571–595. [CrossRef]
14. Shang, H.; Jin, D.; Zhang, T.; Li, S.; Wang, Z.; Zhao, C.; Zhou, Z.; Liu, Z. Permeability evolution of broken coal under triaxial stress. *J. China Coal Soc.* **2019**, *44*, 1066–1075.
15. Li, B.; Chen, S.; Yang, K.; Li, J.; Ren, C. Study on characteristics of shale pore structure and water seepage evolution laws in northern Guizhou. *J. China Coal Soc.* **2020**, *48*, 201–206.
16. Zhu, Z.; Niu, Z.; Que, X.; Liu, C.; He, Y.; Xie, X. Study on Permeability Characteristics of Rocks with Filling Fractures Under Coupled Stress and Seepage Fields. *Water* **2020**, *12*, 2782. [CrossRef]
17. Zhang, T.; Pang, M.; Peng, W.; Liu, N.; Huang, Y. Seepage stability of cemented and fractured coal rock mass under tri-axial stress. *J. Min. Saf. Eng.* **2019**, *36*, 834–840.
18. Zhang, T.; Meng, Y.; Pang, M.; Zhang, L.; Wu, J. Effect of effective stress on the evolution of permeability patterns in perforated fractured coal bodies. *Coal Sci. Technol.* **2023**, *51*, 122–131.
19. Li, S.; Chen, Z.; Miao, X.; Liu, Y. Experimental study on the properties of time-dependent deformation-seepage in water-saturated broken sandstone. *J. Min. Saf. Eng.* **2011**, *28*, 542–547.
20. Yao, Q.; Li, Y.; Li, X.; Yu, L.; Zheng, C. Permeation–strain characteristics and damage constitutive model of coal samples under the coupling effect of seepage and creep. *Int. J. Rock Mech. Min. Sci.* **2024**, *177*, 105729. [CrossRef]
21. Zhao, Y.; Liu, Q.; Tang, L.; Liao, J.; Chang, L.; Wang, X.; Li, Y.; Ren, S. Test study of seepage characteristics of coal rock under various thermal, hydraulic, and mechanical conditions. *Machines* **2022**, *10*, 1012. [CrossRef]
22. Jia, Y.; Cao, Z.; Li, Z.; Du, F.; Huang, C.; Lin, H.; Wang, W.; Zhai, M. Nonlinear evolution characteristics and seepage mechanical model of fluids in broken rock mass based on the bifurcation theory. *Sci. Rep.* **2024**, *14*, 10982. [CrossRef] [PubMed]
23. Hao, D.; Tu, S.; Zhang, L.; Zhao, H.; Xu, S. Experimental study on characteristics of gas seepage in broken coal and rock. *Energy Sci. Eng.* **2024**, *12*, 4737–4752. [CrossRef]
24. Fan, L.; Liu, S. A conceptual model to characterize and model compaction behavior and permeability evolution of broken rock mass in coal mine gobs. *Int. J. Coal Geol.* **2017**, *172*, 60–70. [CrossRef]
25. Shi, W.; Yang, T. A coupled nonlinear flow model for particle migration and seepage properties of water inrush through broken rock mass. *Geofluids* **2020**, *2020*, 1230542. [CrossRef]
26. Liu, Z.; Wang, S.; Yang, H.; Cheng, B.; Han, J. Study on geometry and seepage evolution mechanism of fracture channels in granular filling coal. *Bull. Eng. Geol. Environ.* **2022**, *81*, 418. [CrossRef]
27. Chen, X.; Wang, G.; Chen, H.; Wang, S. Analysis of the effects of coal facture shape factor on water seepage based on computerized tomography (CT) 3D reconstructed artificial fractures. *Fuel* **2023**, *348*, 128571. [CrossRef]
28. Zhang, C.; Zhao, Y.; Tu, S.; Hao, X.; Hao, D.; Liu, J.; Ren, Z. Influence mechanism of particle size on the compaction and breakage characteristics of broken coal mass in goaf. *J China Coal Soc.* **2020**, *45*, 660–670.
29. Zhang, C.; Zhao, Y.; Tu, S.; Zhang, T. Numerical simulation of compaction and re-breakage characteristics of coal and rock samples in goaf. *Chin. J. Geotech. Eng.* **2020**, *42*, 696–704.
30. Ma, Z.; Lan, T.; Pan, Y.; Ma, J.; Zhu, F. Experimental study of variation law of saturated broken mudstone porosity during creep process. *Chin. J. Rock Mech. Eng.* **2009**, *28*, 1447–1454.
31. Yu, B.; Chen, Z.; Feng, M.; Wu, J.; Ding, Q. Microstructure evolution of saturated crushed limestone under lateral confined compression based on CT test. *J. China Coal Soc.* **2017**, *42*, 367–372.
32. Liu, G.; Wang, Y.; Yin, H.; Ding, Y.; Lan, Y.; Tang, D. Effect of pore-throat structure on gas-water seepage behaviour in a tight sandstone gas reservoir. *Fuel* **2022**, *310*, 121901. [CrossRef]
33. Li, Q.; Ma, D.; Zhang, Y.; Liu, Y.; Ma, Y. Insights into controlling factors of pore structure and hydraulic properties of broken rock mass in a geothermal reservoir. *Lithosphere* **2022**, *2021*, 3887832. [CrossRef]
34. Yang, M.; Xu, J.; Gao, J.; Zhang, X.; Liu, J.; Zhang, T.; Ma, J. Study on water seepage law of confined coal body and optimization of water injection parameters. *Fuel* **2023**, *352*, 129152. [CrossRef]

35. Wang, G.; Chen, X.; Wang, S.; Chen, H. Influence of fracture connectivity and shape on water seepage of low-rank coal based on CT 3D reconstruction. *J. Nat. Gas Sci. Eng.* **2022**, *102*, 104584. [CrossRef]
36. Wang, G.; Han, D.; Qin, X.; Liu, Z.; Liu, J. A comprehensive method for studying pore structure and seepage characteristics of coal mass based on 3D CT reconstruction and NMR. *Fuel* **2020**, *281*, 118735. [CrossRef]
37. Chen, Z.; Yu, B. Research progress of seepage mechanics in rock mass affected by mining. *J. Southwest Pet. Univ. Sci. Technol. Ed.* **2015**, *37*, 69–76.
38. Li, S.; Chen, Z.; Miao, X.; Mao, X. Bifurcation of fluid-solid coupling flow in broken rock. *J China Coal Soc.* **2008**, *33*, 754–759.
39. Yu, B.; Pan, S.; Guo, J.; Zhang, Y. Seepage Testing System with Circulating Water Supply for Broken Rock. *Saf. Coal Mines* **2020**, *51*, 137–141.